# MICROSCALE FLOW AND HEAT TRANSFER BETWEEN THE ROTOR AND THE FLANK FOR ROTARY ENGINE

by

***Zhaoju QIN*** *

School of Mechanical Engineering,
North China University of Water Resources and Electric Power,
Zhengzhou, China

Original scientific paper
https://doi.org/10.2298/TSCI190225330Q

*This paper is to investigate microscale flow and transfer between the rotor and the flank for rotary engine. The rotor and flank are simplified to two disks in order to study flow field and temperature field conveniently. The paper takes analysis of steady laminar flow and heat transfer between two disks separated by a gas-filled gap due to machining tolerance. A 3-D multi-physical coupling model is used, involving velocity slip, temperature jump, rarefaction, and dissipation. A solution based on commercial code COMSOL is derived and the results are used to illustrate the effects to velocity field, temperature distribution, disks' torque, and Nusselt number based on the governing parameters. The paper also investigates the effects of different modified Knudsen number on flow field and temperature field.*

Key words: *rotating disks, velocity slip, temperature jump, rotary engine*

## Introduction

A Wankel-type rotary engine due to its planar geometry increases the sealing line and the multiple vertices. A small scale engine cancels some parts in order to reduce the difficulties of manual assembly, including side sealing. Therefore, side sealing has to depend on machining quality for the rotor and the flank. Manufacturing tolerance and surface roughness are not inevitable. So, the gap generated by fabrication tolerance must exist and the gap value varies among certain range. In order to study the mechanism of the flow field, the rotor and flank are simplified to two disks in order to study conveniently.

The problem of flow and heat transfer over two disks is one of the most popular problems of fluid mechanic in the last several decades. When device or space size for flow approaches the molecular mean free path for fluid, changes of flow and heat transfer phenomena lead to a breakdown of macro-solutions due to the increasing predominant position of surface conditions.

The investigation is aimed at flow and heat transfer between two parallel disks. The distinguishing characters of the study are surface velocity slip and temperature jump. The important of heat transfer from a rotating body can be ascertained in cases of various types of machinery [1, 2]. The first solution to the classical problem of rotating disk was obtained by von Karman and Angew [3]. In this work, authors considered the hydrodynamic behavior generated by an infinite disk and gave a formulation. Next, they proposed famous transformations, which reduced the governing PDE to ODE. Their transformations had been widely adopted to study flow problem [4-6].

* Author's, e-mail: qinzhaoju2@126.com

Fluid velocity at a boundary determinates the flow field, because it has been of major concern in fluid mechanics. A commonly accepted model is based on the hypothesis that the fluid velocity is the velocity of the surface it is in contact with. This is referred to as the no-slip velocity condition. Navier [7] and Goldstein [8] proposed velocity slip proportional to surface shearing stress. As systems approach microscopic scales, the well-established continuum laws are broken [9]. In dilute gaseous flow the failure of the continuum description is quantified by the Knudsen number, defined here as the ratio of the molecular mean free path, $\lambda$, to the channel gap, $\delta$. The regime $0 \le \mathrm{Kn} \le 0.1$ is referred to as slip-flow, no-slip is captured by Kn = 0. For Kn > 0 or $\mathrm{Kn} \approx 0.1$, the continuum description is expected to fail [10], and the regime $0.1 < \mathrm{Kn} \le 10$ is referred to as transition regime [11].

Although in the same physical sense as slip in micro-devices, the term *apparent velocity slip* is used to describe an interface velocity in a conjugate two-domain flow through a porous wall. Apparent velocity slip induced by a lubricated disk in a Newtonian fluid was derived [12, 13]. Slip of polymer solutions, emulsions, particle suspensions in viscometers may form a lower-viscosity, depleted layer of liquid [14-16]. Apparent wall slip was first applied on rotating disk by Wein [17]. Characteristic of roughness is considered to give rise to velocity slip. The partial slip condition for rough surface of a single rotating disk was solved by using mathematical model [18].

Temperature jump is another important characteristic in micro/small devices. This is evident from first comprehensive review in Zandergen and Dijkstra [19] to current application on this subject. Hanzik and Bruneau [20] used numerical method to investigate axially symmetric flow of a viscous incompressible fluid between two infinite rotating disks. Szeri *et al.* [21] made experiments to observe velocity flied of water between finite rotating disks with and without through-flow. The flow between two finite rotating disks enclosed by a cylinder was investigated both numerically and experimentally [22]. By means of a combined asymptotic-numerical analysis, the relationship of the axisymmetric flow between large and finite coaxial rotating disks to the von Karman similarity solution was studied [23]. For temperature jump, there are also a lot of related researches. The method of matched asymptotic expansions was used to obtain information about heat transfer from a non-isothermal disk rotating in a quiescent compressible gas by Magyari *et al.* [24]. The heat transfer phenomenon in the steady flow of an incompressible micropolar fluid between a rotating and a stationary disc was examined [25]. Arora and Stokes [26] have been obtained exact numerical solutions for the steady-state axisymmetric flow of an incompressible Newtonian fluid between two parallel infinite rotating disks for different speed ratio and Reynolds number.

In this paper, steady laminar and heat transfer generated by two infinite parallel disks are considered. The lower disk and the upper disk rotates with angular velocity $\Omega$ and s$\Omega$, respectively. The analysis involves velocity slip, temperature jump, rarefaction and dissipation. A solution based on commercial code COMSOL is derived and the results are used to ilustrated the effects to velocity field, temperature distribution, disks' torque, and Nusselt number based on the governing parameters.

## Geometric and mathematic model

### *Problem description*

Figure 1 represents schematically a physical model of two parallel infinite disks with the gap $\delta$. The $\delta$ is determined by machining tolerance. The lower disk and the upper disk rotates with angular velocity $\Omega$ and $s\Omega$, respectively. The parameters can be zero, positive, or negative.

A cylindrical rotating frame ($r$, $\theta$, $z$) is fixed on the lower disk and rotating with it. The velocity components in $r$, $\theta$, $z$ are $^u$, $^v$, $^w$. The lower disk is insulated and the upper disk is maintained at uniform temperature, operating range from 293 K to 550 K. The determination of the flow field and temperature distribution determined the torque required to rotate disks of finite radius and local Nusselt number. Since the lower surface is insulated, heat transfer is solely due to dissipation. Density, viscosity, and thermal conductivity are assumed constant when temperature keeps unchanged. The fluid is assumed to be a methanol and air mixture.

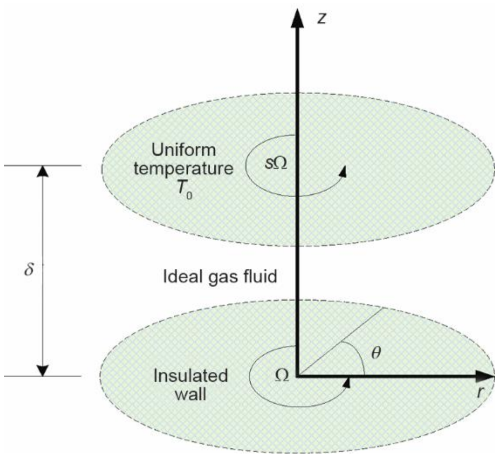


**Figure 1. Disk configuration**

The commercial rotary engine O.S. Pi-49 produced in Japan is chosen to measure surface temperature. The lower disk represents the rotor and the upper disk represents the cover. The rotor temperature is inferred from the surface temperature measured by thermal imager Fluke Ti 55 and heat transfer coefficient based on material properties. The temperature for rotor surface as initial condition is input into the governing equations.

## *Flow field*

### *Governing equations*

The continuity and the Navier-Stokes equations of motion for laminar axis-symmetric flow at cylindrical rotating frame are shown by:

$$\frac{1}{r}\frac{\partial}{\partial r}(ru)+\frac{\partial w}{\partial z}=0 \tag{1}$$

$$u\frac{\partial u}{\partial r}+w\frac{\partial u}{\partial z}-\frac{\upsilon^2}{r}=-\frac{1}{\rho}\frac{\partial p}{\partial r}+\nu\left(\frac{\partial^2 u}{\partial r^2}+\frac{1}{r}\frac{\partial u}{\partial r}-\frac{u}{r^2}+\frac{\partial^2 u}{\partial z^2}\right) \tag{2}$$

$$\frac{u}{r}\frac{\partial}{\partial r}(r\upsilon)+w\frac{\partial \upsilon}{\partial z}=\nu\left(\frac{\partial^2 \upsilon}{\partial r^2}+\frac{1}{r}\frac{\partial \upsilon}{\partial r}-\frac{\upsilon}{r^2}+\frac{\partial^2 \upsilon}{\partial z^2}\right) \tag{3}$$

$$u\frac{\partial w}{\partial r}+w\frac{\partial w}{\partial z}=-\frac{1}{\rho}\frac{\partial p}{\partial r^2}+\nu\left(\frac{\partial^2 w}{\partial r^2}+\frac{1}{r}\frac{\partial w}{\partial r}+\frac{\partial^2 w}{\partial z^2}\right) \tag{4}$$

where $p$ is the pressure and $\nu$ – the kinematic viscosity.

### *Boundary conditions*

The tangential and radial velocity components contain slip on both disks. The Maxwell slip model [27] is used to describe the velocity slip approximately. There is no slip in the axial component. So, the velocity boundary conditions can be given by:

$$u(r,0)=\frac{2-\sigma_u}{\sigma_u}\lambda\frac{\partial u(r,0)}{\partial z},\quad \upsilon(r,0)=\Omega r+\frac{2-\sigma_u}{\sigma_u}\lambda\frac{\partial \upsilon(r,0)}{\partial z}$$

$$w(r,0)=0, \quad u(r,\delta)=-\frac{2-\sigma_u}{\sigma_u}\lambda\frac{\partial u(r,\delta)}{\partial z}$$

$$\upsilon(r,\delta)=s\Omega r-\frac{2-\sigma_u}{\sigma_u}\lambda\frac{\partial \upsilon(r,\delta)}{\partial z}, \quad w(r,\delta)=0$$

$$u(0,z)=0, \quad \upsilon(0,z)=0, \quad \frac{\partial w(0,z)}{\partial r}=0$$

where $\lambda$ is the molecular free path and $\sigma_u$ – the experimentally determined tangential momentum accommodating coefficient.

### *Temperature field*

*Governing equations*

The energy equation is:

$$\rho c_p\left(u\frac{\partial T}{\partial r}+w\frac{\partial T}{\partial z}\right)=k\left(\frac{\partial^2 T}{\partial r^2}+\frac{1}{r}\frac{\partial T}{\partial r}+\frac{\partial^2 T}{\partial z^2}\right)+u\Phi \tag{5}$$

where $\Phi$ is the dissipation function, given by:

$$\Phi=2\left(\frac{\partial u}{\partial r}\right)^2+2\left(\frac{u}{r}\right)^2+2\left(\frac{\partial w}{\partial z}\right)^2+\left(\frac{\partial \upsilon}{\partial r}-\frac{\upsilon}{r}\right)^2+\left(\frac{\partial \upsilon}{\partial z}\right)^2+\left(\frac{\partial u}{\partial z}+\frac{\partial w}{\partial r}\right)^2 \tag{6}$$

*Boundary conditions*

Temperature discontinuity referred to as temperature jump occurs at non-insulated surfaces in micro-channels. The Smoluchowski model for gases relates the temperature jump to the temperature gradient at the surface [27]. In this paper an insulated lower disk and an upper disk maintained at uniform temperature, $T_0$, are considered. The boundary conditions for this case are:

$$\frac{\partial T(r,0)}{\partial z}=0, \quad T(r,\delta)=T_0-\frac{2-\sigma_T}{\sigma_T}\frac{2\gamma}{1+\gamma}\frac{\lambda}{\mathrm{Pr}}\frac{\partial T(r,\delta)}{\partial z}, \quad \frac{\partial T(r,z)}{\partial z}=0$$

where Pr is Prandtl number, $\gamma$ – the specific heats ratio, and $\sigma_T$ – the energy accommodating coefficients. The $\sigma_T$ is uncertain like $\sigma_u$. They are nearly identical for air [28].

## Similarity transformation

### *Flow field*

Following von Karman's solution to the single infinite rotating disk, variables transform the governing partial differential equations to ordinary differential equations [29]:

$$\zeta=\frac{z}{\delta}, \quad u=\Omega r\frac{\mathrm{d}H(\zeta)}{\mathrm{d}\zeta}, \quad \upsilon=\Omega rG(\zeta), \quad w=-2\Omega\delta G(\zeta), \quad \frac{p}{\rho}=\Omega^2\delta^2P(\zeta)+\frac{1}{2}\beta\,\Omega^2r^2 \tag{7}$$

where $\beta$ is constant. The similarity variables in eq. (7) automatically satisfy continuity eq. (1). After similarity transformation, the Navier-Stokes eqs. (2)-(4), become:

$$\frac{1}{\mathrm{Re}}\frac{\mathrm{d}^2G}{\mathrm{d}\zeta^3}+2H\frac{\mathrm{d}^2H}{\mathrm{d}\zeta^2}-\left(\frac{\mathrm{d}H}{\mathrm{d}\zeta}\right)^2+G^2=\beta \tag{8}$$

$$\frac{1}{\mathrm{Re}}\frac{\mathrm{d}^2G}{\mathrm{d}\zeta^3}-2G\frac{\mathrm{d}H}{\mathrm{d}\zeta}+2H\frac{\mathrm{d}G}{\mathrm{d}\zeta}=0 \tag{9}$$

$$\frac{\mathrm{d}P}{\mathrm{d}\zeta}+\left(\frac{1}{\mathrm{Re}}\frac{\mathrm{d}^2G}{\mathrm{d}\zeta^3}+2H\frac{\mathrm{d}G}{\mathrm{d}\zeta}\right)=0 \tag{10}$$

where Re is the Reynolds number, defined:

$$\mathrm{Re}=\frac{\Omega\delta^2}{\nu} \tag{11}$$

Based on similarity variables transformation, boundary conditions 1-6 transform to:

$$\frac{\mathrm{d}H(0)}{\mathrm{d}\zeta}=\mathrm{Kn}\frac{2-\sigma_u}{\sigma_u}\frac{\mathrm{d}^2H(0)}{\mathrm{d}\zeta^2}=\mathrm{Kn}^*\frac{\mathrm{d}^2H(0)}{\mathrm{d}\zeta^2}$$

$$G(0)=1+\mathrm{Kn}\frac{2-\sigma_u}{\sigma_u}\frac{\mathrm{d}G(0)}{\mathrm{d}\zeta}=1+\mathrm{Kn}^*\frac{\mathrm{d}G(0)}{\mathrm{d}\zeta},\qquad H(0)=0$$

$$\frac{\mathrm{d}H(1)}{\mathrm{d}\zeta}=-\mathrm{Kn}\frac{2-\sigma_u}{\sigma_u}\frac{\mathrm{d}^2H(1)}{\mathrm{d}\zeta^2}=-\mathrm{Kn}^*\frac{\mathrm{d}^2H(1)}{\mathrm{d}\zeta^2}$$

$$G(1)=s-\mathrm{Kn}\frac{2-\sigma_u}{\sigma_u}\frac{\mathrm{d}G(1)}{\mathrm{d}\zeta}=s-\mathrm{Kn}^*\frac{\mathrm{d}G(1)}{\mathrm{d}\zeta},\qquad H(1)=0$$

where Kn is Knudsen number defined:

$$\mathrm{Kn}=\frac{\lambda}{\delta} \tag{12}$$

and $\mathrm{Kn}^*$considering the Kn and tangential momentum accommodating coefficient is a modified Knudsen number defined:

$$\mathrm{Kn}^*=\mathrm{Kn}\frac{2-\sigma_u}{\sigma_u} \tag{13}$$

The Kn and $(2-\sigma_u)/\sigma_u$ always appear together in the flow field, so the paper takes the product of Knudsen number and $(2-\sigma_u)/\sigma_u$ as a single parameter $\mathrm{Kn}^*$. When $\sigma_u = 1$ occurs, $\mathrm{Kn}^*$ is equal to Knudsen number.

### *Disk torque*

The torque is needed to drive the disk to rotate. For a disk of finite radius, $r$, the torque can be given by:

$$\mathscr{T}=2\pi\int_0^r\tau_{2\theta}r\mathrm{d}r=-2\pi\mu\int_0^r\frac{\partial\upsilon}{\partial z}r\mathrm{d}r \tag{14}$$

*Disk power*

The product of tangential shearing force and tangential disk velocity determine disk power due to velocity slip. Since force and velocity are related to radial distance, disk power requires integration of the product over the radial distance, $\xi$. The dimensionless power $\mathscr{P}^*(\xi,0)$ for the lower disk and the upper disk $\mathscr{P}^*(\xi,1)$ can be given by eq. (7), respectively.

$$\mathscr{P}^*(\xi,0)=\frac{\mathscr{P}(\xi,0)}{0.5\mu\,\Omega^2\delta^3\xi^4} \tag{15}$$

$$\mathscr{P}^*(\xi,1)=\frac{\mathscr{P}(\xi,1)}{0.5\mu\,\Omega^2\delta^3\xi^4} \tag{16}$$

### *Temperature field*

The dimensionless variables and similarity transformation are defined based on the analysis of no-temperature jump case [30]:

$$\theta(\xi,\zeta)=\frac{c_p}{\Omega^2\delta^2}(T-T_0) \tag{17}$$

$$\xi=\frac{r}{\delta} \tag{18}$$

$$\theta(\xi,\zeta)=M(\zeta)+\xi^2N(\zeta) \tag{19}$$

*Maximum temperature*

The temperature of the lower disk $\theta(\xi,0)$ is acquired by eq. (23). This is the maximum fluid temperature, given by eq. (20):

$$\theta(\xi,0)=M(0)+\xi^2N(0) \tag{20}$$

*Nusselt number*

According to the definition, the Nusselt number of the upper disk can be given:

$$\mathrm{Nu}=\frac{h(r,\delta)\delta}{k} \tag{21}$$

The heat transfer coefficient, $h$, is calculated by equating Fourier's law with Newton's law of cooling.

## Solution

The paper takes method of multi-physical field coupling to analyze steady laminar flow and heat transfer between two disks based on code COMSOL. The size of mesh cells determines the total number of mesh cells, which significantly affects the computation time. Thus, for time and cost saving purpose, fewer cells and larger mesh cell size are preferred, as long as the accuracy of simulating physical property changes are not too much compensated. In order to generate better grid, the geometry is split into five domains as shown in fig. 2. In order to study the grid independent, the elements number chosen are 42190, 53376, and 76458, respectively. The results suggest that the temperature and velocity have no obvious change when the elements number is up to 53376. Basic parameters are show in tab. 1.

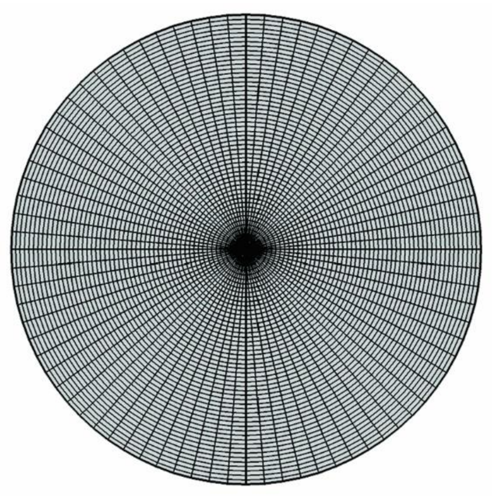

**Figure 2. The mesh grid of disk**

**Table 1. Basic parameters**

| Parameter | Value |
|---|---|
| Thermal conductivity | 0.0404 W/mK |
| Ratio of specific heats | 1.5 |
| Dynamic viscosity | $2.6 \cdot 10^{-5}$ Pa.s |
| Kinematic viscosity | $3.48 \cdot 10^{-5}$ m$^2$/s |
| Density | 0.747 kg/m$^3$ |
| Heat capacity at constant pressure | 1800 J/kgK |
| Upper temperature | 502 K |

## Results and discussion

### *Velocity*

Figure 3 represents velocity field for different Kn$^*$ at 5000 rpm. The characteristic of velocity field for different Kn$^*$ can be shown by fig. 3 when the speed constants at 5000 rpm.

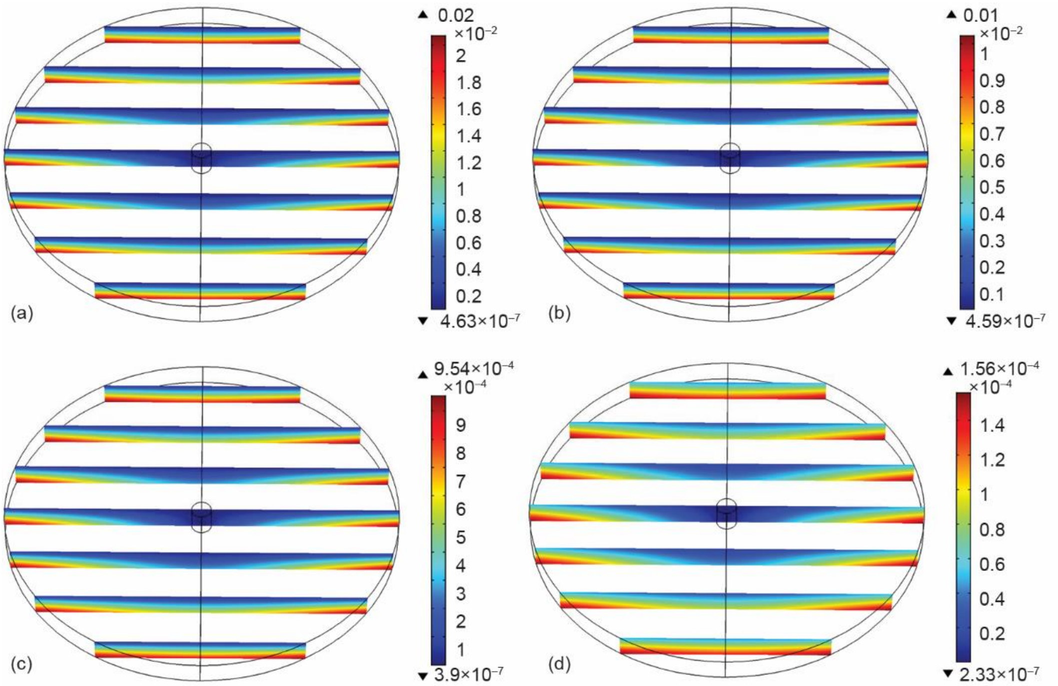


**Figure 3. The velocity field for different Kn$^*$ at 5000 rpm; (a) Kn$^*$ = 0, (b) Kn$^*$ = 0.01, (c) Kn$^*$ = 0.1, (d) Kn$^*$ = 0.5** (*for color image see journal web site*)

The velocity field trend is basically the same for all the Kn*. The velocity decreases with increased Kn*. The velocity at Kn* = 0.5 almost decreases by 100 times compared with the one at Kn* = 0.

The radius of the disks are chosen as $1.25\cdot10^{-5}$ m. Because the cover is static, $s$, is equal to 0. Figure 4 shows that axial velocity increases at radial direction for the same value of $z$, Kn*, speed. An increase in Kn* can come about as a result of a decrease in axial velocity due to the increase in velocity slip. Figure 5 depicts the effect of the slip on the velocity magnitude at $z$- direction when $\delta$ = 0.5 μm and $r = 8\cdot10^{-6}$ m. The decreasing rate of velocity magnitude is slowed down when Kn* changes from 0 to 0.3 due to increasing slip. Figures 4 and 5 indicate that the existence of slip in the direction of $r$ and $z$ leads to small curve gradient for Kn* = 0.3.

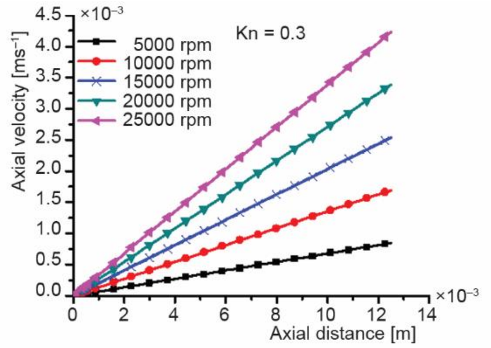


**Figure 4. Axial velocity for different speed at Kn***

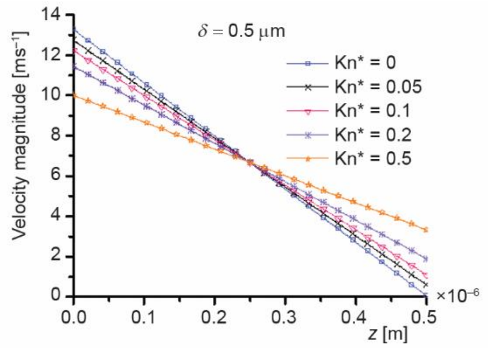


**Figure 5. Velocity for different Kn***

That is, velocity initial value at $z$ = 0 decreases for the increasing in Kn* and velocity value at $z$ = 0.5 increases for the increasing in Kn*. The Kn* = 0 represents continuous fluid. Figure 4 shows that velocity increases with the increased speed. The results indicate positive correlation between the slip and the speed.

Figure 6 shows that velocity increases with the rise of the speed at Kn* = 0.1. The presented results show that the velocity variation tendency to the speed is less than the one to the Kn*. The results indicate that the velocity due to the variation of the Kn* is more apparent relative to the influence of the speed.

### *Disk torque*

Figures 7 and 8 show the influence of Re, $\delta$, speed, and Kn* on the lower and upper disk torques, $T^*(0)$ and $T^*(1)$, respectively. There are two ways to change Reynolds number. One is change of the speed and the other is change of the spacing between disks. The value of s is selected as 0 according to actual engine. It means the upper disk is stationary. Rarefaction and the effect of modified coefficient, $\sigma_u$, are investigated by five values of Kn* ranging from 0 to 0.3. Figure 7 shows that the relation between $T^*(0)$ and Reynolds number due to the speed for $\delta$ = 0.5 μm. The lower increases as the small Reynolds number is on the increase for all values of Kn*.

The upper disk torque shows a reverse trend to that for the lower disk torque. However, the value of torque for the upper and lower disk increases monotonically with Reynolds number. In order to examine Kn*, it is necessary to increase Kn* and velocity slip, which results in an increase in rarefaction and a decrease in $\sigma_u$. A decease in $T^*(0)$ and $T^*(1)$ with increasing Kn* is accordance with expectation.

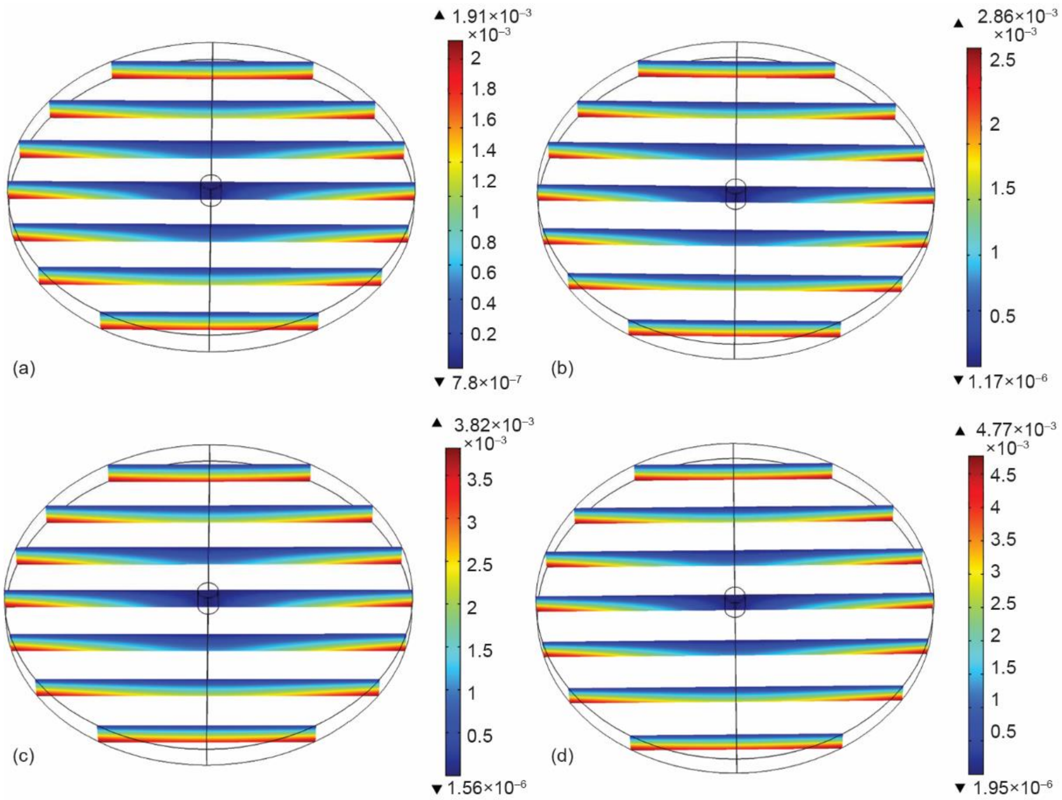


**Figure 6. The velocity field for different speed at Kn$^*$ = 0.1; (a) rotation speed = 10000 rpm, (b) rotation speed = 15000 rpm, (c) rotation speed = 20000 rpm, (d) rotation speed = 25000 rpm** (*for color image see journal web site*)

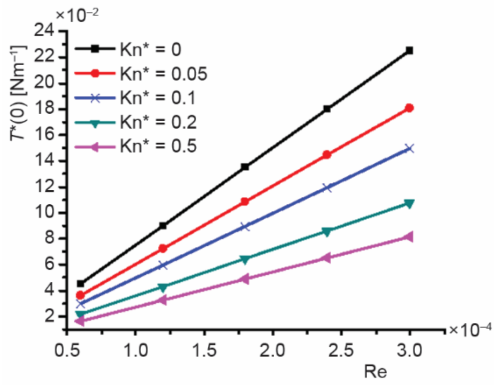


**Figure 7. The lower torque**

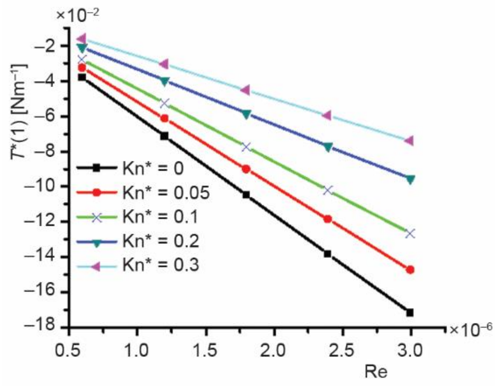


**Figure 8. The upper torque**

### *Surface temperature*

Figure 9 presents the temperature jump for the middle surface between the lower disk and the upper disk at 25000 rpm. The common characteristic is that temperature distribution diffuse from the center to the outer. It is also shown that the temperature jump focuses on the central region. The jump area is reduced and more concentrated from $Kn^* = 0.5$ to $Kn^* = 0.05$. However, the value of the temperature jump become smaller.

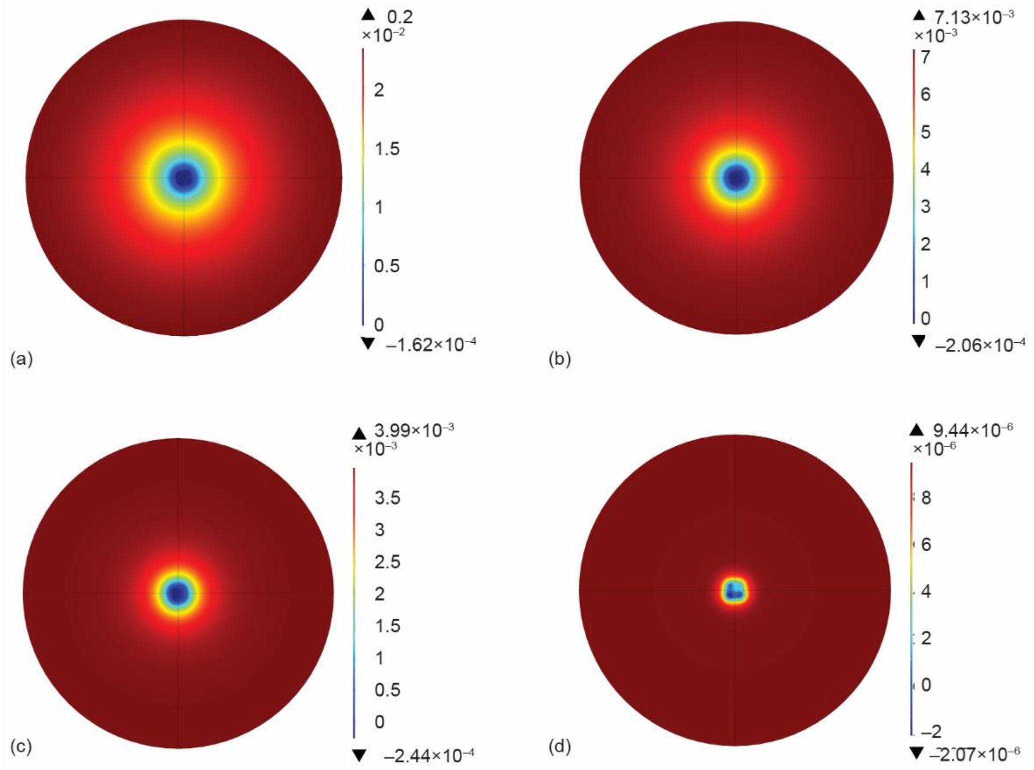


**Figure 9. The temperature jump for different $Kn^*$ at 25000 rpm; (a) $Kn^* = 0.5$, (b) $Kn^* = 0.2$, (c) $Kn^* = 0.1$, (d) $Kn^* = 0.05$** (*for color image see journal web site*)

Figure 10 presents the temperature jump on the middle surface between the lower disk and the upper disk at different rotational speed for $Kn^* = 0.1$. The temperature jump happens on the center and the temperature decreases at small region.

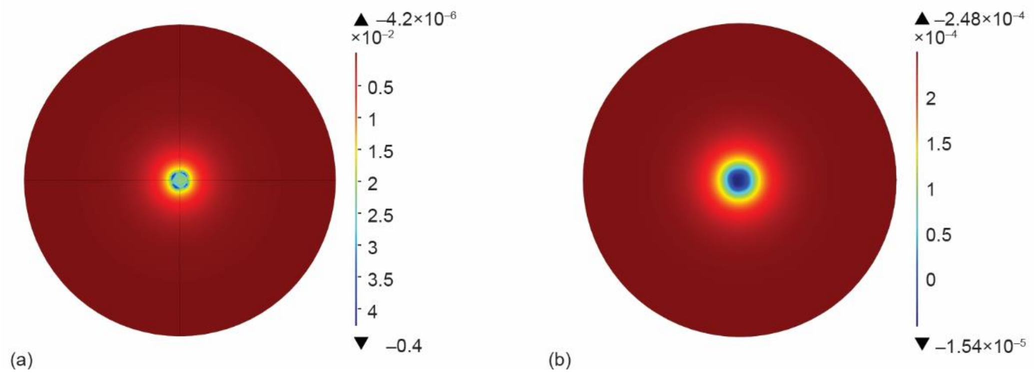


**Figure 10. The temperature jump for different speed at $Kn^* = 0.1$; (a) speed = 5000 rpm, (b) speed = 15000 rpm** (*for color image see journal web site*)

### *Nusselt number*

Figure 11 presents the Nusselt number for the values of $Kn^*$ from 0.05 to 0.3 at different speed. The Nusselt number changes non-linearly with $\xi$, reaching an asymptotic value, which depends on Reynolds number (speed), and $Kn^*$. The Nusselt number happens oscillation and oscillation gradually tend to be gentle from $Kn^* = 0.05$ to $Kn^* = 0.3$. The position occurred vibration back continually until $Kn^*$ at 0.3. Increasing $Kn^*$ decreases the Nusselt number. Influence of speed on Nusselt number is vanished at $Kn^* = 0.3$. The change law of the Nusselt number for the high speed is more stable than that of low speed.

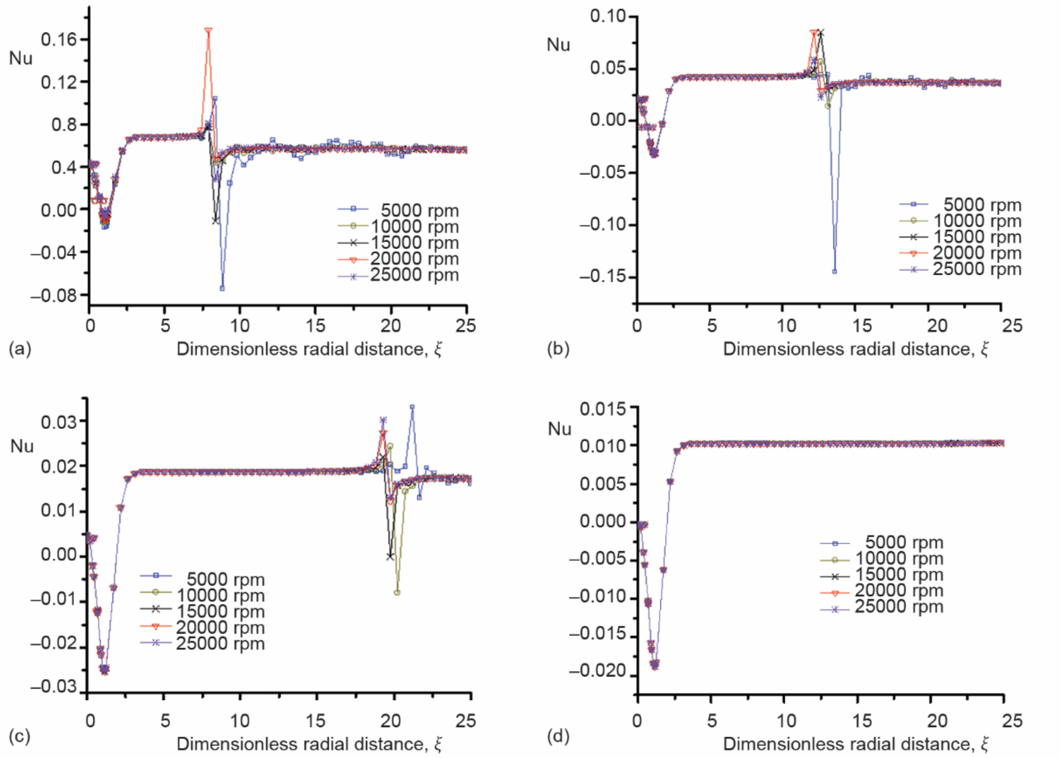


**Figure 11. The Nusselt number for different $Kn^*$; (a) $Kn^* = 0.05$, (b) $Kn^* = 0.1$, (c) $Kn^* = 0.2$, (d) $Kn^* = 0.3$** (*for color image see journal web site*)

## Conclusions

- The simulation to the flow field and temperature distribution for rotating disks separated by a micro-gap is obtained using multi-physical coupling method. The two transformed non-linear fourth order coupled ODE are solved numerically.
- Dimensionless disks torque depend on two parameters: $Kn^*$ and Re. Increasing $Kn^*$ decreases the lower disk torque. The effect of the parameters on the lower disk torque is monotonic.
- Dimensionless temperature and local Nusselt number depend on four parameters: Kn, Re, Pr, and $\gamma^*$.

- In general, temperature rise due to dissipation is small. For the conditions shown in fig. 7 the maximum jump is 0.04 K. Relatively high temperature rise is associated with large $\Omega$.
- The local Nusselt number at the upper disk changes greatly with the radial distance, $\xi$, reaching an asymptotic value which depends on Re and $Kn^*$. This phenomenon is analogous to the fully developed asymptotic Nusselt numbers characteristic of macrochannels. The variation of the asymptotic value with Re and Kn does not follow a well defined pattern.

## References

[1] Rashidi, M. M., *et al.*: Double Diffusive Magnetohydrodynamic (MHD) Mixed Convective Slip Flow along a Radiating Moving Vertical Flat Plate with Convective Boundary Condition, *PLoS ONE, 9* (2014), 10, ID 109404
[2] Owen, J. M., Rogers, R. H., Flow and Heat Transfer in Rotating Disc System, Rotor-Stator System, Research studies, Taunton, vol. 1, Wiley, New York, USA, 1989
[3] Von Karman, T., Angew, Z., Uber laminare und turbulente reibung. *Math. Mech., 1* (1921), 1, pp. 233-325
[4] Muthtamilselvan, M., Renuka, A., Nanofluid Flow and Heat Simultaneously Induced by Two Stretchable Rotating Disks Using Buongiorno's Model, *MMMS, 14* (2018), 5, pp. 1115-1128
[5] Knyazev, D. V., Axisymmetric Flows of an Incompressible Fluid between Movable Rotating Disks, *Fluid Dynamics, 46* (2011), 4, pp. 558-564
[6] Turkyilmazoglu, M., Flow and Heat Simultaneously Induced by Two Stretchable Rotating Disks, *Physics of Fluids, 28* (2016), 4, ID 043601
[7] Navier, C. L. M. H. Mémoires de l.'Académie, Royale des Sciences de l'Institut de France 1823, 1, pp. 414-416.
[8] Goldstein, D., In *Modern Developments in Fluid Machanics*, 2nd ed.; Volume II, pp. 4.3-4.6, Clarendon Press; Publisher: Oxford, England, 1938
[9] Ho, C. M., Tai, Y. C. Micro-Electro-Mechanical Systems (MEMS) and Fluid Flow, *Annu. Rev. Fluid Mech. 30* (1998), 1, pp. 579-612
[10] Haeri, S., Shrimpton, J. S., A New Implicit Fictitious Domain Method for the Simulation of Flow in Complex Geometries with Heat Transfer, *J. Comput. Phys., 237* (2013), Mar., pp. 21-45
[11] Nicolas, G. H., Olga, S., Constant-Wall-Temperature Nusselt Number in Micro and Nano-Channels, *ASME, 124* (2002), 2, pp. 356-364
[12] Anderson, H. I., Valnes, O. A., Slip-Flow Boundary Conditions for Non-Newtonian Lubrication Layers, *Fluid Dyn. Res., 24* (1999), 4, pp. 211-217
[13] Anderson, H. I., Rousselet, M., Slip Flow over a Lubricated Rotating Disk, *Int. J. Heat Mass Transfer, 27* (2006), 2, pp. 329-335
[14] Moomey, M., Wang, C. Y., The Flow due to a Rough Rotating Disk, *ZAMP, 55* (2004), Mar., pp. 235-246
[15] Tretheway, D. C., Meinhart, C. D., A Generating Mechanism for Apparent Fluid Slip in Hydrophobic Micro-channels, *Phys. Fluid, 16* (2004), 5, pp. 1509-1515
[16] Barns, H. A., A Review of the Slip (Wall Depletion) of Polymer Solutions, Emulsion and Particle Suspensions in Viscometers: Its Cause, Character, and Cure, *J. Non-Newton. Fluid, 56* (1995), 3, pp. 221-251
[17] Wein, O., Viscometric Flow under Apparent Wall Slip in Parallel-Plate Geometry, *J. Non-Newton. Fluid, 126* (2005), 2-3, pp. 105-114
[18] Miklavcic, M., Wang, C. Y., The Flow due to a Rough Rotating Disk, *ZAMP, 55* (2004), 2, pp. 235-246
[19] Zandbergen, P. J., Dijkstra, D., von Karman Swirling Flows, *Annu. Rev. Fluid Mech., 19* (1987), pp. 465-491
[20] Honzík, P., Bruneau, M., Acoustic Fields in Thin Fluid Layers between Vibrating Walls and Rigid Boundaries: Integral Method, *Acta Acustica United with Acustica, 101* (2015), 4, pp. 859-862
[21] Szeri, A. Z., *et al.,* Flow between Rotating Disks. Part I: Basic Flow, *J. Fluid Mech., 134* (1983), Sept., pp. 103-131
[22] Heise, M., *et al.,* Co-Rotating Taylor-Couette Flow Enclosed by Stationary Disks, *J. Fluid Mech., 716* (2013), Feb., R4
[23] Brady, J. F., *et al.,* Slip at a Uniformly Porous Boundary: Effect on Fluid Flow and Mass Transfer, *J. Eng. Math., 26* (1992), 4, pp. 481-492

[24] Magyari, E., *et al.*, Heat and Mass Transfer Characteristics of the Self-Similar Boundary-Layer Flows Induced by Continuous Surfaces Stretched with Rapidly Decreasing Velocities, *Heat Mass Tran., 38* (2001), 1-2, pp. 65-74
[25] Agarwal, R. S., Dhanapal, C., Heat Transfer in Micropolar Fluid Flow between Two Coaxial Discs – One Rotating and the Other at Rest, *Int. J. Sci., 27* (1989), 2, pp. 181-186
[26] Arora, R. C., Stokes, V. K., On the Heat Transfer between Two Rotating Disks, *Int. J. Heat Mass Transfer, 15* (1995), 11, pp. 2119-2132
[27] Gad-el-Hak, M., Flow Physics, in: *The MEMS Handbook* (ed. Gad-el-Hak, M.), CRC Press, Boka Raton, Fla., USA, 2005, pp. 676-680
[28] Zohar, Y., *Heat Convection in Micro Ducts*, Kluwer Academic Publishers, Boston, Mass., USA, 2005
[29] Karniadakis, G., *et al., Microflows and Nanoflows*, Springer, New York, USA, 2005
[30] Roozemond, P. C., *et al.*, Modeling Flow-Induced Crystallization in Isotactic Polypropylene at High Shear Rates. *J. Rheol., 59* (2015), 3, pp. 613-642

Paper submitted: February 25, 2019
Paper revised: July 23, 2019
Paper accepted: July 31, 2019